ROBOTIC WHEELCHAIR CONTROL CONSIDERING USER COMFORT

Modeling and Experimental Evaluation

Razvan Solea and Urbano Nunes
ISR - Institute of Systems and Robotics, Department of Electrical and Computer Engineering
University of Coimbra, 3030-290, Coimbra, Portugal

Keywords: Users comfort, sliding-mode control, human head-neck complex model, intelligent wheelchair.

Abstract: This paper analyzes the comfort of wheelchair users when a sliding-mode trajectory-tracking controller is used. The transmission of the horizontal (fore-and-aft) vibration to the head-neck complex (HNC) in the seated human body may cause unacceptable discomfort and motion sickness. A double-inverted pendulum model with two degrees of freedom is considered as a model for the HNC. The user comfort is examined not only in the time domain (using the fourth power vibration dose value), but also in the frequency domain (using the cross-spectral density method). For measuring the acceleration of the wheelchair, along the trajectory, an inertial measurement unit was used.

1 INTRODUCTION

Few studies have been performed addressing how dynamic acceleration affects wheelchair's users. A barrier to performing in-depth analysis during the processes of wheelchair design and ride comfort is a lack of wheelchair-acceleration data, measured over time, that vary with the activity of the wheelchair user. Furthermore, little is known about how this dynamic acceleration affects user comfort. Most current literature focus on the vibration exposure of a seated occupant. To this end, standards have been developed by the International Organization for Standardization (ISO) to quantify how much exposure is allowable for various frequencies of exposure. To standardize the methods of data collection for whole-body vibration, the ISO introduced the ISO-2631 (ISO-2631, 1997). The boundaries in ISO-2631 are based on cumulative root-mean-square (rms) amplitude over a single day, specified for frequencies between 1 and 80 Hz.

The human body is a complex dynamic system, the properties of which vary from moment to moment and from one individual to another. From the results of large amount of experimental data, various biomechanical models have been developed to describe the human motion. These models can be grouped as lumped or distributed parameter models. The lumped parameter models consider the human body as several rigid bodies, springs and dampers (Atapourfard et al., 2002), (Atapourfard et al., 2004), (Gurses et al., 2005). Some distributed models treat the spine as a layered structure of rigid elements, representing the vertebral bodies and deformable elements representing the intervertebral disc by the finite elements (Kitazaki and Griffin, 1997).

The dynamic response of seated subjects exposed to vibration has been widely assessed in terms of the driving point impedance, apparent mass and transmissibility (transmission of motion through the human body). The transmission of the acceleration to the head-neck complex (HNC) in the seated human body may be the cause of discomfort and motion sickness in wheelchairs. The seat back, by limiting the horizontal and rotational motion of the trunk, increases the transmission of the trunk horizontal acceleration to the HNC. This may has considerable influence on discomfort.

The present study focuses specifically on the influence of sliding-mode trajectory-tracking (SM-TT) controller action on user comfort. The user comfort is examined not only in the time domain (using the transmissibility parameter), but also in the frequency domain. For measuring accelerations of the wheelchair, a three-dimensional inertial sensor was used. The analysis of user comfort is made in three different situations: i) SM-TT control under odometry navigation; ii) when the odometric data is fused with absolute position data from magnetic markers (using

Solea R. and Nunes U. (2008).
ROBOTIC WHEELCHAIR CONTROL CONSIDERING USER COMFORT - Modeling and Experimental Evaluation.
In *Proceedings of the Fifth International Conference on Informatics in Control, Automation and Robotics - RA*, pages 37-44
DOI: 10.5220/0001487100370044

an EKF-based fusion in the on-line pose estimation); iii) SM-TT control with purposely-incorrectly-tuned parameters.

2 CONTROL OF WHEELED MOBILE ROBOTS

The application of sliding mode control strategies in nonlinear systems has received considerable attention in recent years (Yang and Kim, 1999), (Chwa, 2004), (Chwa et al., 2006), (Solea and Nunes, 2007). A well-studied example of a non-holonomic system is a wheeled mobile robot (WMR) that is subject to the *rolling without slipping* constraint.

In trajectory-tracking, is an objective to control the non-holonomic WMR to follow a desired path, with a given orientation relatively to the path tangent, even when disturbances exist. In the case of trajectory-tracking the path is to be followed under time constraints. The path has an associated velocity profile, with each point of the trajectory embedding spatiotemporal information that is to be satisfied by the WMR along the path. By other words, path tracking is formulated as having the WMR following a virtual target WMR which is assumed to move exactly along the path with specified velocity profile.

2.1 Kinematic Model of a Unicycle-type Mobile Robot

Let the pose of the mobile robot be defined by the vector $q_r = [x_r, y_r, \theta_r]^T$, where $[x_r, y_r]^T$ denotes the robot position on the plane and θ_r the heading angle with respect to the *x*-axis. In addition, v_r denotes the translational velocity of the robot, and ω_r the angular velocity around the vertical axis. For a unicycle WMR rolling on a horizontal plane without slipping, the kinematic model can be expressed by:

$$\begin{bmatrix} \dot{x}_r \\ \dot{y}_r \\ \dot{\theta}_r \end{bmatrix} = \begin{bmatrix} cos\theta_r & 0 \\ sin\theta_r & 0 \\ 0 & 1 \end{bmatrix} \cdot \begin{bmatrix} v_r \\ \omega_r \end{bmatrix} \quad (1)$$

which represents a non-linear system.

Controllability of the system (1) is easily checked using the Lie algebra rank condition for nonlinear systems. However, the Taylor linearization of the system about the origin is not controllable, thus excluding the application of classical linear design approaches.

2.2 Trajectory Tracking Model

Without loss of generality, it can be assumed that the desired trajectory $q_d(t) = [x_d(t), y_d(t), \theta_d(t)]^T$ is generated by a virtual unicycle mobile robot. The kinematic relationship between the virtual configuration q_d and the corresponding reference velocity inputs $[v_d, \omega_d]^T$ is similar to (1). From the error vector (Solea and Nunes, 2007),

$$\begin{bmatrix} x_e \\ y_e \\ \theta_e \end{bmatrix} = \begin{bmatrix} cos\theta_d & sin\theta_d & 0 \\ -sin\theta_d & cos\theta_d & 0 \\ 0 & 0 & 1 \end{bmatrix} \cdot \begin{bmatrix} x_r - x_d \\ y_r - y_d \\ \theta_r - \theta_d \end{bmatrix} \quad (2)$$

we get the error dynamics:

$$\begin{cases} \dot{x}_e = -v_d + v_r \cdot cos\theta_e + \omega_d \cdot y_e \\ \dot{y}_e = v_r \cdot sin\theta_e - \omega_d \cdot x_e \\ \dot{\theta}_e = \omega_r - \omega_d \end{cases} \quad (3)$$

Table 1: ISO 2631-1 Standard.

Overall Acceleration	Consequence
$a_w < 0.315 m/s^2$	not uncomfortable
$0.315 < a_w < 0.63 m/s^2$	a little uncomfortable
$0.5 < a_w < 1 m/s^2$	fairly uncomfortable
$0.8 < a_w < 1.6 m/s^2$	uncomfortable
$1.25 < a_w < 2.5 m/s^2$	very uncomfortable
$a_w > 2.5 m/s^2$	extremely uncomfortable

2.3 Trajectory Planner

A trajectory planner for human-transport robots must generate smooth velocity profiles (linear and angular) with low associated accelerations. The trajectory planning process can be divided into two separate parts. First, a continuous collision-free path is generated. In a second step, called trajectory generation, a velocity profile along the path is determined. A method to generate a velocity profile, respecting human body comfort, for any two-dimensional path in static environments was proposed in (Solea and Nunes, 2007).

Figures 1 - 3 show an example of a planned trajectory using the method described in (Solea and Nunes, 2007) were the goal was to obtain an overall rms acceleration in the range of "not uncomfortable" (see Table 1). The overall rms acceleration is defined as:

$$a_w = \sqrt{k_x^2 \cdot a_{wx}^2 + k_y^2 \cdot a_{wy}^2 + k_z^2 \cdot a_{wz}^2} \quad (4)$$

where a_{wx}, a_{wy}, a_{wz}, are the rms accelerations along *x*, *y*, *z* axes respectively, and k_x, k_y, k_z, are multiplying factors. For a seated person $k_x = k_y = 1.4$, $k_z = 1$. For motion on the x-y plane, $a_{wz} = 0$. The local coordinate system is chosen so that the *x*-axis is the longitudinal trajectory direction, and *y*-axis is the lateral trajectory direction.

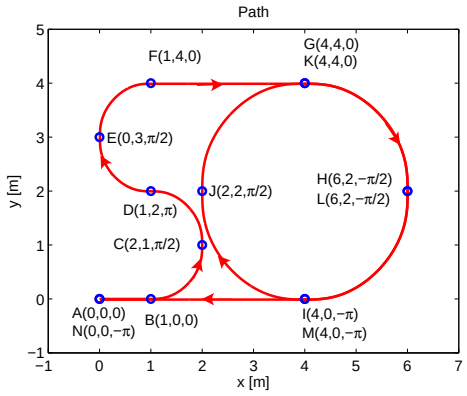

Figure 1: Path example composed by thirteen path segments calculated by the trajectory planner, from the fourteen waypoints A to N.

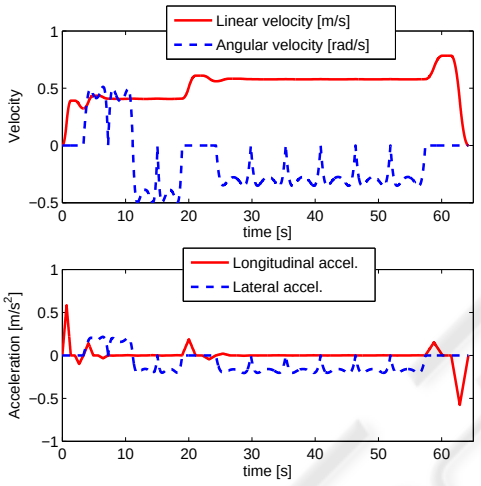

Figure 2: Velocity and acceleration profiles for path depicted in Fig. 1.

The ISO 2631-1 standard (ISO-2631, 1997) (Table 1) relates comfort with the overall rms acceleration, acting on the human body.

Figure 1 shows the generated path, where the larger circles represent the used fourteen waypoints (A, B, ..., N). Each waypoint is defined by a position, in meters, and an orientation, in radians. The generated velocity and acceleration profiles are shown in Fig. 2. As can be observed in Fig.3, the rms overall accelerations, in each path segment, are below the imposed acceleration constraint of $a_{w(i,i+1)} < 0.31 m/s^2$.

2.4 Sliding-mode Controller

The objective of SMC is the same as for classical controllers, i.e., force the output states to follow the desired input states. However, the SMC is a model-based control strategy in which the controller structure and gains are designed based on the system model.

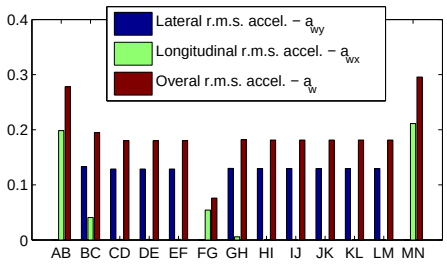

Figure 3: Acceleration rms values for each path segment (AB, BC, ..., MN) of path depicted in Fig. 1.

Uncertainties which exist in real mobile robot applications degrade the control performance significantly, and accordingly, need to be compensated. In (Solea et al., 2006) a SM-TT controller for WMRs is proposed, where trajectory tracking is achieved even in the presence of large initial pose errors and disturbances.

Let us define the sliding surface $s = [s_1\ s_2]^T$ as

$$\begin{aligned} s_1 &= \dot{x}_e + k_1 \cdot x_e, \\ s_2 &= \dot{y}_e + k_2 \cdot y_e + k_0 \cdot sgn(y_e) \cdot \theta_e. \end{aligned} \tag{5}$$

where k_0, k_1, k_2 are positive constant parameters, x_e, y_e and θ_e are the trajectory-tracking errors defined in (3). If s_1 converges to zero, trivially x_e converges to zero. If s_2 converges to zero, in steady-state it becomes $\dot{y}_e = -k_2 \cdot y_e - k_0 \cdot sgn(y_e) \cdot \theta_e$. For $y_e < 0 \Rightarrow \dot{y}_e > 0$ if only if $k_0 < k_2 \cdot |y_e| / |\theta_e|$. For $y_e > 0 \Rightarrow \dot{y}_e < 0$ if only if $k_0 < k_2 \cdot |y_e| / |\theta_e|$. Finally, it can be known from s_2 that convergence of y_e and $\dot{y}_e$ leads to convergence of θ_e to zero. Using the reaching law defined in (Gao and Hung, 1993)

$$\begin{aligned} \dot{s} &= -Q \cdot s - P \cdot sgn(s) \\ Q &= diag\,[q_1, q_2], \quad q_i > 0, \\ P &= diag\,[p_1, p_2], \quad p_i > 0, \ i = 1,2 \\ sgn(s) &= [sgn(s_1), sgn(s_2)]^T \end{aligned} \tag{6}$$

together with (5), and after some mathematical manipulation, we get the commands for trajectory-tracking controller:

$$\begin{aligned} \dot{v}_c = \frac{1}{cos\theta_e}(&-q_1 s_1 - p_1 sgn(s_1) - k_1 \dot{x}_e - \\ &- y_e \dot{\omega}_d - \dot{y}_e \omega_d + v_r \dot{\theta}_e sin\theta_e + \dot{v}_d). \end{aligned} \tag{7}$$

$$\begin{aligned} \omega_c = \frac{1}{v_r cos\theta_e + k_0 sgn(y_e)}(&-q_2 s_2 - p_2 sgn(s_2) - \\ &- k_2 \dot{y}_e - \dot{v}_r sin\theta_e + x_e \dot{\omega}_d + \dot{x}_e \omega_d) + \omega_d. \end{aligned} \tag{8}$$

The SM-TT architecture with a on-line robot's pose estimator, fusing odometry with absolute position data, as described in (Lopes et al., 2007), is depicted in Fig. 4.

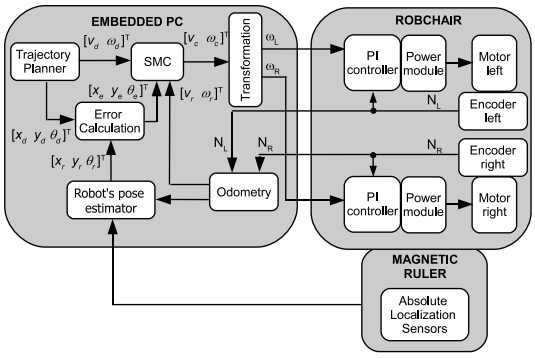

Figure 4: SM-TT control architecture with a robot's pose estimator, fusing odometry and absolute position data.

RobChair has a two-level control architecture (see Fig. 4). High-level control algorithms (including reference motion generation) are written in *C* and run with a sampling time of $T_s = 50$ ms on a embedded PC, which also provides a user interface with real-time visualization and a simulation environment. The PC communicates through a CAN bus with several devices. Wheel velocity commands,

$$\omega_R = \frac{v_c + \frac{L}{2} \cdot \omega_c}{R}, \quad \omega_L = \frac{v_c - \frac{L}{2} \cdot \omega_c}{R} \qquad (9)$$

where R is radius of the drive wheels and L the distance between drive wheels, are sent to the PI controllers, and encoder measures N_R and N_L are received in the robot's pose estimator for odometric computations.

The low-level control layer is in charge of the execution of the wheels velocity control. For each wheel, a microcontroller implements a digital PI with a cycle time of $T_c = 5$ ms. Two power amplifiers drive the motors with PWM voltage.

3 HUMAN HEAD-NECK COMPLEX MODEL AND EVALUATION OF COMFORT

In general, comfort while riding depends not only on the amplitude, but also on the frequency of wheelchair vibrations and accelerations. Oscillations have influence on users comfort and may affect users health. Moreover, natural frequency of the wheelchair and human organ is strongly related with the user's uncomfort while riding.

3.1 Model of Head-neck Complex

A double-inverted pendulum model with two degrees-of-freedom is considered for the HNC model (Fig. 5).

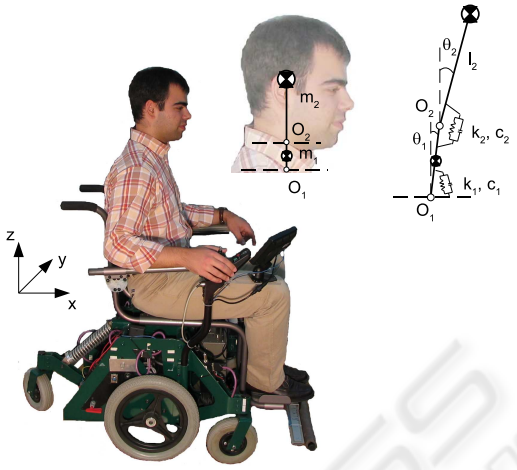

Figure 5: Human head-neck model.

One of the centers of rotation of the model was assumed to be at C7-T1 (O_1 in Fig. 5), and the other at C0-C1 (O_2 in Fig. 5) of the cervical spine. Two lumped masses, indicating the mass of the neck and the mass of the head, were considered in the model. The center of mass of the neck was assumed to be exactly at the mid-point of the two centers of rotation. Moreover, the center of mass of the head was assumed to be exactly over the center of mass of the neck and the center of rotation (Fig. 5). The equation of motion using generalized coordinates can be expressed as:

$$M(q)\ddot{q} + C(q,\dot{q})\dot{q} + Kq + G(q) = Q_q \qquad (10)$$

where: $q = \begin{bmatrix} \theta_1 \\ \theta_2 \end{bmatrix}$, $Q_q = 0$,

$M(q) = \begin{bmatrix} M_{11} & M_{12} \\ M_{21} & M_{22} \end{bmatrix}$

$M_{11} = m_1 l_1^2 + m_2 L_1^2 + J_1$

$M_{12} = m_2 L_1 l_2 cos(\theta_1 - \theta_2)$

$M_{21} = m_2 L_1 l_2 cos(\theta_1 - \theta_2)$

$M_{22} = m_2 l_2^2 + J_2$

$C(q,\dot{q}) = \begin{bmatrix} c_1 + c_2 & C_{12} \\ C_{21} & c_2 \end{bmatrix}$

$C_{12} = m_2 L_1 l_2 sin(\theta_1 - \theta_2)\dot{\theta}_2 - c_2$,

$C_{21} = -m_2 L_1 l_2 sin(\theta_1 - \theta_2)\dot{\theta}_1 - c_2$,

$K = \begin{bmatrix} k_1 + k_2 & -k_2 \\ -k_2 & k_2 \end{bmatrix}$

$G(q) = \begin{bmatrix} -(m_2 L_1 + m_1 l_1)\ddot{x}cos(\theta_1) \\ -m_2 l_2 \ddot{x} cos(\theta_2) \end{bmatrix}$

In our study, the user characteristic elements, shown in Table 2 (from (Atapourfard et al., 2002)), were used to model the dynamic behavior of the human HNC.

Table 2: Characteristics of user's elements.

Element	Neck	Head
Length of segment $L_i[m]$	0.080	0.138
Center of gravity $l_i[m]$	0.040	0.069
Mass $m_i[kg]$	1.01	4.22
Moment of Inertia $J_i[kgm^2]$	0.0011	0.210
Spring constant $k_i[Nm/rad]$	14.04	10.29
Damping constant $c_i[Nms/rad]$	0.347	0.230

3.2 Time-domain Calculations

The fourth power vibration dose value (VDV) is primarily a measurement procedure used to report the relative severity of complex oscillation exposures, being preferred to other measures due to its use of the duration and variability of the motion:

$$VDV = \left\{ \int_0^T [a_w(t)]^4 \cdot dt \right\}^{\frac{1}{4}} \tag{11}$$

in units of $ms^{-1.75}$, where the frequency-weighted acceleration is defined by $a_w(t)$, and T is the duration of an experiment. VDV was selected over the difference between the peak accelerations and acceleration rms parameter. The problem with the peak-to-peak value is that it only represents one instance in time, rather than the entire signal. Furthermore, the peak-to-peak parameter does not accurately represent oscillatory motion. The problem with the rms value is that it is independent of the duration of the signal, and is designed to describe oscillatory motions.

According to the EU Directive on mechanical vibration (European-Parliament and the Council of the European Union, 2002) the average limit value of VDV is $9.1ms^{-1.75}$ and the upper limit is $21ms^{-1.75}$.

The transmissibility (T_r) is defined as the output VDV divided by the input VDV,

$$T_r = \frac{VDV_{output}}{VDV_{input}} \tag{12}$$

The transmissibility defines the performance of the wheelchair in terms of the amplification or attenuation of the vibration that is transmitted to the occupant. A value less than unity indicates that the accelerations were attenuated by the combination of wheelchair and human, whereas a value great than unity indicates an amplification of accelerations by the wheelchair-human system.

3.3 Frequency-domain Calculations

Given the input, wheelchair acceleration, and the output, acceleration obtained from the HNC model, the transfer function is usually calculated using the cross-spectral density (CSD) method defined as:

$$H_{CSD}(f) = \frac{CSD_{input-output}(f)}{PSD_{input}(f)} \tag{13}$$

where $CSD_{input-output}(f)$ is the CSD of the input and output, and $PSD_{input}(f)$ is the power spectral density (PSD) of the input. The advantage of using the CSD method is that the function generates the phase of the response and also only includes data at the input and output that are correlated, thus reducing the effects of noise in the measurement system.

4 EXPERIMENTAL RESULTS

In order to validate the applicability of the sliding-mode controller for trajectory-tracking, real experiments have been performed using RobChair (intelligent platform developed in ISR-UC (Pires and Nunes, 2002), (Lopes et al., 2007)). RobChair, shown in Fig.6, has two differentially driven rear wheels and two passive castor front wheels. There is also a fifth rear wheel connected to the back of the wheelchair with a damper used for stability. It is powered by two 12-V batteries (60 Ah) and reaches a maximum speed of 7 Km/h. It has been equipped, in ISR-UC, with several devices such as: two power driver modules, which provide an independent control of each motor, optical encoders, laser range finders, an inertial sensor and a magnetic sensing ruler, developed at ISR-UC, that is able to perform a robust detection of magnetic markers (Lopes et al., 2007). Figure 7 presents a block diagram of the actual hardware control architecture. The current implementation of the framework is based on Linux as its underlying real-time operating system. The component-based software selected for the proposed software framework is GenoM (Generator of Modules) (Fleury et al., 1997), which is an environment for description and implementation of software components.

An embedded PC is responsible for giving some degree of intelligence to the robot. This computer is connected to distributed devices through fieldbuses. The platform is connected to external devices through a wireless link. This connection allows the implementation of a distributed architecture, which exhibits the possibility and capability to extend our single robot to other perspectives, like multi-robot cooperation, its integration in intelligent environments, etc.

All the distributed devices, connected through CAN, use a base printed circuit board, containing a microchip micro-controller (μC), as described in (Maia, 2004). A custom communication protocol,

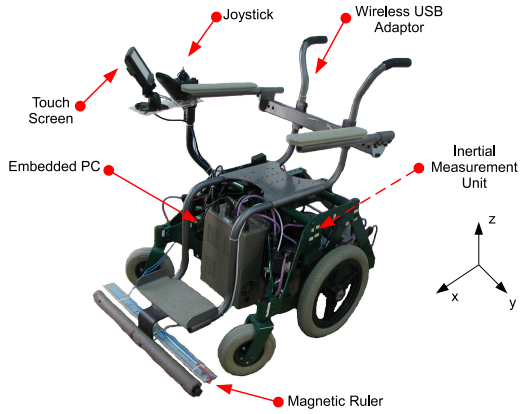

Figure 6: RobChair platform.

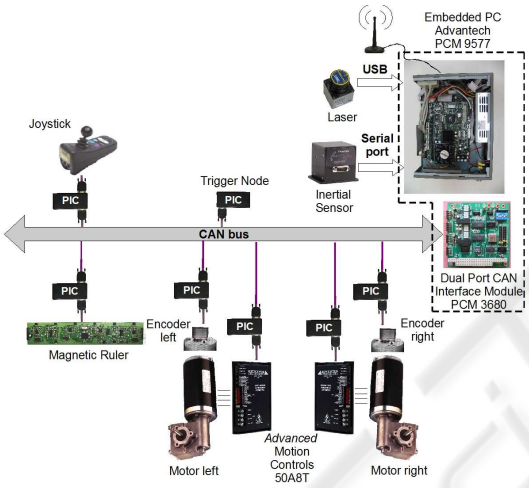

Figure 7: RobChair hardware architecture.

based on the time-triggered protocol paradigm, was designed and implemented. All events are synchronized by a message, sent from a Synchronization Micro-Controller Unit (Trigger Node, in Fig. 7), that synchronizes the other Micro-Controller Units, and defines the control loop time reference.

The odometric data provided by the wheel encoders is fused with the data from magnetic markers. The extended Kalman filter (EKF) was chosen for the fusion process (Bento et al., 2005). This navigation technology, based on sensing magnetic markers, is well suited when high precision navigation and robustness is required, and it can be used to complement other navigation systems, such as GPS.

The inertial sensor RGA300CA-100 (Crossbow) was used for measuring the wheelchair accelerations in three orthogonal directions.

Experimental results of the SM-TT controller using the planned path presented in Fig 1, are shown

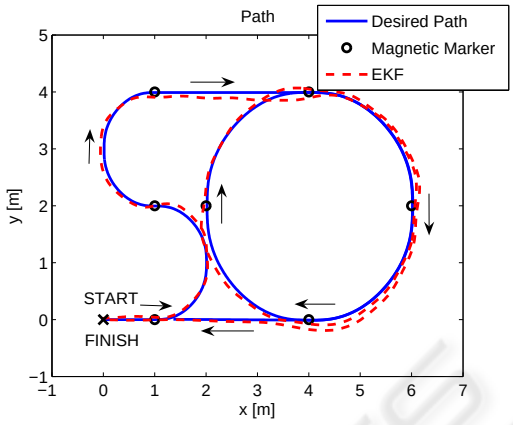

Figure 8: Experimental sliding-mode trajectory-tracking control using an EKF-based fusion in the on-line pose estimation.

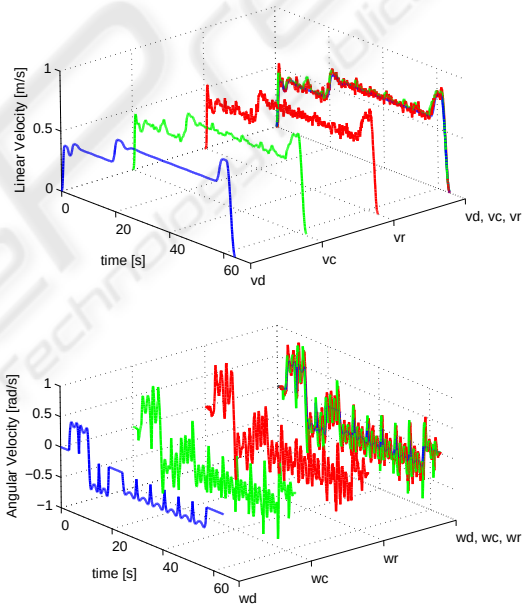

Figure 9: Desired (v_d, ω_d), command (v_c, ω_c) and real (v_r, ω_r) linear/angular velocities for SM-TT control under magnetic-markers navigation (case B).

in Figs. 8- 10. Figure 9 shows desired, command and real linear and angular velocities for SM-TT control under magnetic-markers navigation. Corrections in the pose after each magnetic marker detection provokes an error signal that is efficiently dealt by the SM-TT controller, and rapidly the tracking errors converge to zero (see Fig. 10).

The analysis of user comfort is made in three different situations:

- case A: SM-TT control under odometry navigation;

Table 3: Experimental Results.

Case	No	VDV_x RobChair	VDV_x Head	T_r	RMS accel. RobChair	Max. accel RobChair	RMS accel. Head	Max. accel Head
	I	2.9219	1.3826	0.4732	0.3287	1.5686	0.1656	0.7286
A	II	2.7634	1.3429	0.4859	0.3191	1.4988	0.1589	0.7307
	III	2.7177	1.2802	0.4710	0.3187	1.5590	0.1510	0.8210
average		2.8010	1.3352	0.4767	0.3222	1.5421	0.1585	0.7601
	I	2.9481	1.4408	0.4887	0.3538	1.2853	0.1797	0.7100
B	II	3.2946	1.5707	0.4767	0.3663	1.7635	0.1856	0.7988
	III	3.0318	1.4860	0.4901	0.3629	1.4136	0.1828	0.7755
average		3.0915	1.4992	0.4852	0.3610	1.4875	0.1827	0.7614
C	-	11.4623	5.4607	0.4764	1.5185	4.1708	0.7039	2.2210

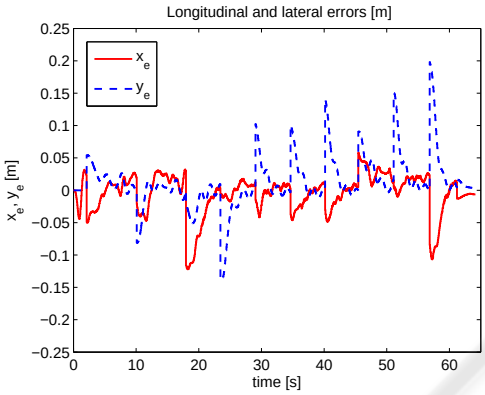

Figure 10: Longitudinal and lateral errors for SM-TT control under magnetic-markers navigation (case B).

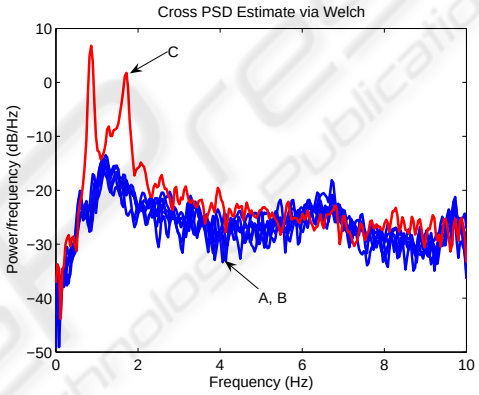

Figure 11: Cross-spectal density functions for all experiments.

- case B: SM-TT control under magnetic-markers navigation (odomeric data is fused, using an EKF-based fusion, with absolute position data from magnetic markers detection);
- case C: SM-TT control with purposely-incorrectly-tuned parameters.

The experimental data of all three cases are summarized in Table 3. Three experimental trials were executed in cases *A* and *B*. The table shows the vibration dose value (VDV), transmissibility (T_r), root mean square accelerations (RMS) and maximum values (Max). The results of columns "RMS accel. Robchair" and "Max. accel. RobChair" concern the acceleration results obtained by the inertial sensor; and the "RMS accel. Head" and "Max. accel. Head" were obtained from the model of head-neck complex (10). The overall rms acceleration of head (along the x axes) in cases *A* and *B* are in range of "not uncomfortable", but in case *C* is in range of "uncomfortable" (see Table 1 and equation (4)).

Each experiment was made for the same trajectory (see Fig. 1). The time domain VDV values obtained in cases *A* and *B* are below the limit value of $9.1ms^{-1.75}$, only in case *C*, VDV values are above that limit. As can be observed from Table 3, the transmissibility tends to be under unity, suggesting that the vibrations are attenuated.

Figure 11 shows cross-spectral density values for all experiments. The maximum of H_{CSD} magnitude occurs in case *C*, and the corresponding frequencies are between $0.8 - 1.8Hz$. When the magnitude of H_{CSD} increases, the user comfort decreases.

5 CONCLUSIONS

Wheelchair is exposed to vibration coming not only from a variety of different road surface but also from the command of the wheelchair (manually - using Joystick or automated - using different type of controllers). The paper analyzes the comfort of wheelchair users when a SM-TT controller is used. The user comfort is examined not only in time domain (using the fourth power VDV), but also in frequency

domain (using the cross-spectral density method). Outdoor experiments, using RobChair with SM-TT controller were performed. The experimental tests presented in this paper are representative of the average performance of the controllers. We had summarized our acquired experience in general observations that can be useful guidelines for implementation of the same control strategies in other type of mobile robots.

ACKNOWLEDGEMENTS

This work was supported in part by ISR-Coimbra and Portuguese Technology and Science Foundation (FCT), under contract NCT04: POSC/EEA/SRI/58016/2004. R.Solea acknowledges a PhD research fellowship from FCT.

REFERENCES

Atapourfard, M., Ishihara, T., and Inooka, H. (2002). The influences of trunk horizontal vibration to the head-neck complex. In *SICE02*, pages 1053–1058, Osaka.

Atapourfard, M., Ishihara, T., and Inooka, H. (2004). Identification of the head-neck complex in response to trunk horizontal vibration. *Biological Cybernetics*, 90(6):418–426.

Bento, L., Nunes, U., Moita, F., and Surrecio, A. (2005). Sensor fusion for precise autonomous vehicle navigation in outdoor semi-structured environments. In *8th IEEE International Conference on Intelligent Transportation Systems (ITSC'05)*, pages 245–250, Vienna.

Chwa, D. (2004). Sliding-mode tracking control of nonholonomic wheeled mobile robots in polar coordinates. *IEEE Transactions on Control Systems Technology*, 12(4):637–644.

Chwa, D., Hong, S., and Song, B. (2006). Robust posture stabilization of wheeled mobile robots in polar coordinates. In *17th International Symposium on Mathematical Theory of Networks and Systems*, pages 343–348, Kyoto.

European-Parliament and the Council of the European Union (2002). *On the minimum health and safety requirements regarding the exposure of workers to the risks arising from physical agents (vibration).* Official Journal of the European Communities, Directive 2002/44/EC.

Fleury, S., Herrb, M., and Chatila, R. (1997). Genom: A tool for the specification and the implementation of operating modules in a distributed robot architectures. In *IEEE of the International Conference on Intelligent Robots and Systems*, pages 842–848, Grenoble.

Gao, W. and Hung, J. (1993). Variable structure control of nonlinear systems: A new approach. *IEEE Transactions on Industrial Electronics*, 40(1):45–55.

Gurses, S., Dhaher, Y., Hain, T., and Keshner, E. (2005). Perturbation parameters associated with nonlinear responses of the head at small amplitudes. *CHAOS*, 15(2):023905.

ISO-2631 (1997). *Mechanical vibration and shock - Evaluation of human exposure to whole body vibration - Part 1: General requirements.* International Organization for Standardization.

Kitazaki, S. and Griffin, M. (1997). A modal analysis of whole-body vertical vibration using a finite element model of the human body. *Journal of Sound and Vibration*, 200(1):83–103.

Lopes, A. C., Moita, F., Nunes, U., and Solea, R. (2007). An outdoor guidepath navigation system for AMRs based on robust detection of magnetic markers. In *12th IEEE International Conference on Emerging Technologies and Factory Automation*, pages 989–996, Patras.

Maia, R. (2004). Movimento de robots moveis com rodas de tracao diferencial: modelacao e controlo do sistema motriz. Master's thesis, Universidade de Coimbra (in portuguese), Coimbra.

Pires, G. and Nunes, U. (2002). A wheelchair steered through voice commands and assisted by a reactive fuzzy-logic controller. *Journal of Intelligent and Robotic Systems*, 34:301–314.

Solea, R. and Nunes, U. (2007). Trajectory planning and sliding-mode control based trajectory-tracking for cybercars. *Integrated Computer-Aided Engineering, IOS Press*, 14(1):33–47.

Solea, R., Nunes, U., and Filipescu, A. (2006). Trajectory planning and sliding-mode control for WMR trajectory-tracking and path-following respecting human comfort travel. In *7th Portuguese Conference on Automatic Control - CONTROLO'2006*, Lisbon.

Yang, J. and Kim, J. (1999). Sliding mode control for trajectory tracking of nonholonomic wheeled mobile bobots. *IEEE Transactions on Robotics and Automation*, 15(3):578–587.